Reaction energetics of Hydrogen on the Si(100) surface revisited: A periodic many-electron theory study

Theodoros Tsatsoulis,[1,2] Sung Sakong,[3] Axel Groß,[3] and Andreas Grüneis[1,2,*]

[1] *Max Planck Institute for Solid State Research, Heisenbergstrasse 1, 70569 Stuttgart, Germany*
[2] *Institute for Theoretical Physics, Vienna University of Technology, Wiedner Hauptstrasse 8-10, 1040, Vienna, Austria*
[3] *Institute of Theoretical Chemistry, Ulm University, Albert-Einstein-Allee 11, 89081 Ulm, Germany*

(Dated: August 22, 2018)

We report on a many-electron wavefunction theory study for the reaction energetics of hydrogen dissociation on the Si(100) surface. We demonstrate that quantum chemical wavefunction based methods using periodic boundary conditions can predict chemically accurate results for the activation barrier and the chemisorption energy in agreement with experimental findings. These highly accurate results for the reaction energetics enable a deeper understanding of the underlying physical mechanism and make it possible to benchmark widely used density functional theory methods.

Introduction.—Reactions of gas-phase molecules on surfaces play an important role in many physical and chemical processes. Along a surface reaction path, the energetics of the combined molecule–surface system varies significantly according to the rearranged chemical bonds featuring charge transfer, covalent bonding, and weak van der Waals interactions. Arrhenius relation indicates a small error in the activation energy can cause a large change of the reaction rate. Thus a many-electron theory able to describe a wide range of exchange and correlation effects in molecules, solids, and molecule–surface systems simultaneously is required to estimate a reaction scheme with chemical accuracy (1 kcal/mol). The computational method of choice for such problems is density functional theory (DFT) due to its good trade-off between accuracy and computational cost [1–3]. However, several shortcomings exist in the most widely used approximate exchange-correlation functionals [4]. Density functionals based on parametrizations that achieve accurate results only for either solids or gas-phase molecules, introduce systematic errors in combined molecule–surface systems [5]. Many local and semi-local density functional approximations underestimate reaction barriers, often due to the self-interaction error [4, 6]. The lack of chemically accurate benchmark results for molecule–surface systems limits our understanding of the various origins of error in currently available density functionals. High level *ab-initio* wavefunction theories, such as the coupled cluster (CC) method, predict molecular reactions as well as properties of solids with chemical accuracy [7–10]. However, owing to their large computational cost these methods have so far only been applied to small cluster models or used in embedding techniques when applied to surfaces [11–14]. A careful validation against periodic high level wavefunction methods is still missing to date.

In this Letter we consider a prototypical molecule–surface reaction: the dissociative adsorption of molecular hydrogen on the Si(100) surface [15–26]. Previous studies identify two reaction paths of dissociative H_2 adsorption, termed the intra- (H2*) and inter-dimer (H2) pathways, as shown in Fig. 1. Along both reaction paths, the stretch of H–H bond is accompanied by a significant modification of the characteristic buckled Si-dimer configuration in the vicinity of the molecule [26–29]. These structural modifications induce delicate changes to the electronic structure. DFT methods based on generalized gradient approximation (GGA) capture the changes in the electronic exchange and correlation effects poorly along the reaction paths and result in too small adsorption barriers and reaction energies compared to experiments [16, 20, 21]. Quantum Monte Carlo (QMC) and quantum chemistry methods using finite clusters predict adequate adsorption barriers for both pathways, however, reaction energies are overestimated [17, 23, 24]. In previous DFT and high level correlated calculations, H_2 adsorption is hindered by the smallest barrier through the H2 pathway, and the reaction occurs via a pairing mechanism [25, 26].

Here, we present a periodic quantum chemical description of the reaction using a recently implemented periodic CC theory, applicable to molecule–surface systems [30–32]. We show that activation and reaction energies are calculated to within chemical accuracy compared to experimental values. Most interestingly, it becomes clear that the adsorption barriers for the H2* and H2 pathways are very similar, in contrast to previous findings. We will demonstrate that the main source of error of DFT-GGA is the self interaction error leading to an incorrect ground state density for the H2 path.

Electronic-structure calculations.—We employ periodic slabs for all density functional and wavefunction based calculations. A Si(100)-2×2 surface with 8-layers is used, terminated with hydrogen atoms to passivate dangling bonds at the bottom layer. The two reaction pathways were obtained using the Perdew-Burke-Ernzerhorf (PBE) exchange-correlation functional [33] employing the nudged elastic band (NEB) method [34] and the cor-

responding structures are shown in Fig. 1. We use the same geometries for the initial, transition, and final states for all methods. This allows for a direct comparison of the different levels of theory. Contributions of vibrational zero-point energies (ZPE) are included in all calculations and were taken from Ref. [23]. All calculations involve a plane-wave basis within the full potential projector-augmented-wave method (PAW) as implemented in the VASP code [35–39]. In all calculations the $1s$ electronic states of the H atoms and the $3s$ and $3p$ states of the Si atoms were treated as valence states. A $4\times4\times1$ k-mesh was employed for all DFT calculations. We have explored the accuracy of several density functional approximations covering all five rungs of the Jacob's ladder of DFT proposed by Perdew and Schmidt [40]. Periodic wavefunction based calculations were also performed using a plane-wave basis within the PAW framework. Hartree–Fock (HF) calculations were converged within the plane-wave basis. For second order perturbation theory (MP2), CC singles and doubles (CCSD) and perturbative triples (CCSD(T)), as well as the random phase approximation (RPA), we employ a set of atom-centered Gaussian-type functions based on Dunning's correlation consistent polarized Valence Quadruple Zeta basis set augmented with diffuse functions (aVQZ) [41–43], mapped onto a plane-wave representation [44], to construct the unoccupied one-electron states. A $4\times4\times1$ k-mesh was employed for the twist-averaging procedure [32] used in the CCSD calculations, whereas the remaining finite size error of the correlation energy was corrected for using an interpolation technique of the structure factor on a plane-wave grid [32]. CCSD(T) results were obtained as correction to CCSD using the Γ-point approximation. See Supplemental Material at [] for further technical details.

Results.—Figure 2 shows the calculated reaction energetics for H_2 on the (100) surface of Si at different levels of theory, together with the experimental estimates and the corresponding error depicted by the shaded area. The results are also summarized in Table. II. We first consider the reaction energy (E_{rxn}) shown in the top panel and we will turn to the discussion of barrier heights later. The reaction energy is defined as $E_{rxn} = E_{initial} - E_{final}$, where the corresponding final and initial structures are shown in Fig. 1. The experimental estimate for the reaction energy is 1.9±0.3 eV [22]. The local-density approximation (LDA) constitutes the lowest rung of Perdew's Jacob's ladder of DFT methods. Reaction energies computed in the LDA are approximately 0.3 eV too small compared to the experimental estimate. The PBE functional is one of the most extensively used GGA functionals which represent the second rung of the Jacob's ladder and noticeably underestimates the reaction energy without any improvement compared to LDA. The meta-GGA functionals lie on the third rung and utilize the kinetic energy together with the electron density and its gradient. The strongly constrained and appropriately normed

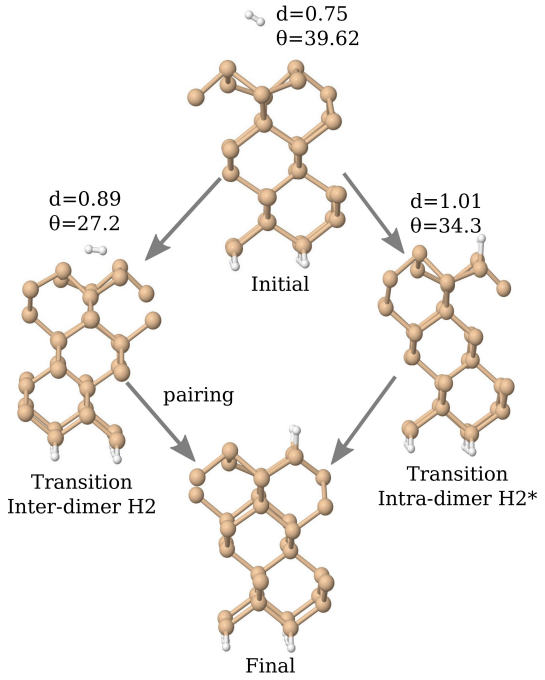

FIG. 1. Intra- ($H2^*$) and inter-dimer (H2) reaction pathways at low coverage (one H_2 molecule per two Si dimers). d denotes the bond length of the H_2 molecule in Å whereas θ the buckling angle of the Si dimers in degree.

(SCAN) [45, 46] meta-GGA density functional significantly improves the reaction energy (E_{rxn}^{SCAN} =1.97 eV), demonstrating its ability to describe diversely bonded molecules and materials such as the H–Si system accurately. Hybrid GGAs provide an improved description of covalent, hydrogen and ionic bonding by mixing non-local exact exchange with GGA exchange. B3LYP [47], PBE0 [48], and HSE06 [49] yield a reaction energy with a similar accuracy as SCAN. The good agreement between the hybrids and the SCAN functional confirms that meta-GGAs can yield reaction energies at the same level of accuracy yet at lower computational cost. As a method of the fifth rung of Perdew's Jacob's ladder we examine the RPA. The RPA correlation energy is fully non-local and seamlessly includes electronic screening as well as long-range dispersion interactions [50, 51]. The chemisorption energy in the RPA is, however, underestimated compared to hybrid-GGA and meta-GGA functionals, in agreement with a well known underestimation of binding energies [52]. Overall we find that the predicted DFT results for the reaction energy are improving as one moves from lower to higher rungs with the exception of the RPA. However, we attribute the underestimated RPA reaction energy to the neglect of post-RPA corrrections and a lack of self-consistency.

We now switch from DFT to the wavefunction based hierarchy for treating electronic correlation. HF theory, approximating the many-electron wavefunction by a sin-

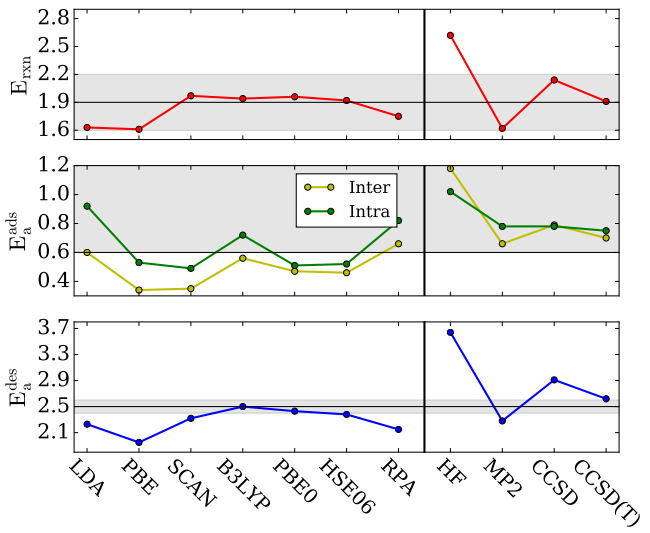

FIG. 2. Reaction energetics for H_2 dissociation on the Si(001) surface calculated at different levels of theory. The calculated reaction energies (E_{rxn}) adsorption (E_a^{ads}) and desorption (E_a^{des}) barriers for H_2 dissociative adsorption on Si(100) surface. The black lines represent the experimental estimate while the shaded region the error. All energies given in eV.

gle Slater determinant, overestimates the reaction energy by as much as 0.7 eV compared to experiment. In passing we note that this is in contrast to atomization energies of molecules and cohesive energies of solids, which are usually underestimated by HF [53, 54]. Adding correlation effects at the level of MP2 theory over-corrects HF and yields a reaction energy of 1.62 eV, almost 0.3 eV smaller than the experimental estimate. We assign this overcorrection of MP2 to the small band gap of the Si surface. The more sophisticated CCSD theory overestimates the experimental reaction energy by 0.25 eV. Adding the perturbative triples correction (T) to CCSD yields a reaction energy that is very close to hybrid DFT results and the experimental estimate. This demonstrates the ability of the wavefunction based hierarchy to yield systematically improvable and chemically accurate chemisorption energies for molecules on periodic surfaces. However, we note that at lower levels of theory, the DFT based methods exhibit a significantly better trade-off between accuracy and computational cost.

Having confirmed experimental measurements for the chemisorption energy using accurate electronic structure theories, we now seek to discuss the activation barrier height for the dissociation, which is defined by $E_a^{ads} = E_{transition} - E_{initial}$. Establishing accurate estimates of barrier heights is more difficult compared to reaction energies for theory as well as experiment. Transition states often exhibit strong electronic correlation effects that can only be treated accurately using higher levels of theory. Furthermore experimental measurements of adsorption barriers are usually lower bounds and do not allow to determine directly whether the reaction proceeds via the H2 or H2* mechanism. Adsorption barriers for both pathways are depicted in the middle panel of Fig. 2, alongside the experimental lower bound of 0.6 eV [21]. LDA yields a barrier of 0.6 eV and 0.92 eV for the H2 and H2* pathway, respectively. The difference in the barriers between the two pathways is considerable. Noteworthy, LDA does not vastly underestimate the activation energies, but yields rather adequetly high barriers for both mechanisms. PBE underestimates the reaction barriers and yields in agreement with LDA a larger barrier for the H2* pathway. We observe the same trend for the SCAN functional. Although the description of the reaction energy is much improved, SCAN fails to ameliorate the errors in the reaction barriers predicted by GGA, yielding a too low barrier for the H2 path and the same difference between the barriers of the two pathways. Interestingly, LDA predicts much larger activation energies than GGA, challenging the trend LDA<GGA observed for adsorption barriers of molecular reactions [55]. Similar results, however, have been reported for activation energies of gas-phase reactions [56]. Hybrid functionals mix exact exchange with commonly-used density functionals and partly cancel the spurious self-interaction error. In the case of H_2 on Si(100) hybrid functionals do improve the description of the reaction barrier. B3LYP yields a barrier height of 0.56 eV for the H2 path, whereas PBE0 and HSE06 yield barriers of 0.47 eV and 0.46 eV respectively. For the H2* mechanism B3LYP predicts a barrier 0.16 eV higher than the H2 one, whereas PBE0 and HSE06 yield barriers only 0.04 and 0.06 eV higher than the H2 pathway, respectively. The RPA yields significantly higher barriers compared to PBE when combined with exact exchange computed with PBE orbitals. However, we note that the H2 path is still favored by RPA with a barrier of 0.66 eV compared to 0.82 eV of the H2* path. The results discussed above illustrate convincingly a lack of systematic improvability in the obtained estimates of barrier heights as one moves from lower to higher levels of approximate DFT based methods. Furthermore, errors in activation energies may vary sigificantly with the employed density functional. Therefore reliable predictions for the barrier height and the relative stability of the considered transition states are not possible. Nevertheless, the considered system provides a realistic and insightful scenario to further develop and improve upon the computationally efficient DFT based methods.

We now turn to the discussion of wavefunction based *ab-initio* calculations for the barrier. HF theory yields barriers larger than 1 eV for both pathways. In contrast to DFT based findings, HF favors the H2* path over the H2 one by 0.16 eV. In order to better understand the difference between HF and DFT, we consider the different paths as a competition between stretching the H_2 molecule and flattening the Si dimers of the surface. In Fig. 1 the hydrogen bond in the H2 transition state is

0.89 Å, compared to 1.01 Å of the H2* one, whereas the dimers buckling angle is 27.2° for the former and 34.3° for the latter transition state. In order to see why HF favors the H2* path we need to consider the energy cost between the buckled and symmetric configurations of the Si dimer reconstruction. This energy difference per dimer is 250–260 meV for LDA and GGA, in contrast to 544 meV for HF. We identify the energy penalty for flattening the dimers as the main difference between HF and DFT methods, owing to a large extent on the metallic nature of the symmetric Si dimer configuration. MP2 theory reverses the preference of the two pathways. Furthermore, the MP2 adsorption barrier for the H2 transition state is 0.66 eV while for the H2* is 0.78 eV. Due to the smaller band gap of the H2 transition state MP2 overcorrects HF, hence it favors the lower band gap H2 reaction pathway. CCSD theory yields barriers for the two reaction mechanisms that are practically degenerate. Specifically, the H2 transition state barrier is 0.79 eV and the H2* 0.78 eV. In agreement with experiment the inclusion of perturbative triples, CCSD(T), yields activation barriers of 0.70 eV for the H2 transition and 0.75 eV for the H2* one, retaining the picture of two approximately degenerate barriers of CCSD to within chemical accuracy.

The picture emerging from the results discussed above is qualitatively different within the methods we examine. The two barriers are approximately degenerate using the more sophisticated CCSD and CCSD(T) theories, in contrast to LDA, PBE and SCAN functionals, where the H2 path is favored. Hybrid functionals remedy partly the self-interaction error and thus yield barriers that differ less than the GGA and LDA ones. An exception is B3LYP, where although the barriers are higher in energy, the H2 path is favored by 0.16 eV. The reason is that part of the exchange-correlation functional is based on a mixture of LDA and GGA rather than solely on GGA as in PBE0 and HSE06. Thus B3LYP contains part of the LDA errors and deficiencies, hence the higher barriers and the larger difference between the two pathways. Barriers for the two mechanisms based on the RPA also differ significantly. We associate the discrepancy between the CCSD(T) barriers and the RPA ones with the use of PBE orbitals for the RPA calculations as opposed to the HF ones for CCSD(T). It is likely that a sizeable fraction of the error exists already in the original DFT functional, leading to an overestimation of the H2 barrier. In order to get more insight into the disagreement of CC methods and DFT based methods, we performed non-self-consistent calculations for the activation barriers of the two mechanisms at the level of DFT-PBE using HF orbitals. The results are shown in Table. II. We observe that when HF orbitals are employed for DFT-PBE calculations the H2 barrier is appreciably higher, whereas the H2* one remains almost the same. The difference between the two barriers is 0.04 eV in close agreement with the accurate CCSD(T) and hybrid DFT results. This is partly due to the cancellation of the density driven one-electron self-interaction error [57], and similar results have been obtained for simple molecular reaction barriers and adsorption energies [58, 59].

TABLE I. Adsorption barriers for the two pathways, alongside desorption and reaction energies. Desorption energies correspond to the energetically lowest path, whereas reaction energies to the intra-dimer (H2*) geometry, since it is energetically the lowest configuration. ZPE corrections assumed for all calculations(identical for both pathways). All energies are reported in eV.

	E_a^{ads}[H2]	E_a^{ads}[H2*]	E_a^{des}	E_{rxn}
LDA	0.60	0.92	2.23	1.62
PBE	0.34	0.53	1.95	1.61
PBE@HF	0.46	0.50	2.13	1.76
SCAN	0.35	0.49	2.32	1.97
B3LYP	0.56	0.72	2.50	1.94
PBE0	0.47	0.51	2.43	1.96
HSE06	0.46	0.52	2.38	1.92
RPA	0.66	0.82	2.16	1.75
HF	1.18	1.02	3.79	2.62
MP2	0.66	0.78	2.28	1.62
CCSD	0.79	0.78	2.92	2.18
CCSD(T)	0.70	0.75	2.62	1.91
QMC [24]	(0.09)0.63	(0.05)0.75	(0.09)2.91	(0.05)2.20
Expt. [15, 21, 22]	> 0.6	> 0.6	(0.10)2.50	(0.30)1.90
ZPE [23]	+0.09	+0.09	−0.11	−0.20

Finally, we examine the desorption mechanisms for the reaction. The desorption barrier is defined as $E_a^{des} = E_{transition} - E_{final}$. QMC corrections using finite clusters [24] predict that none of the H2 or H2* mechanisms are compatible with temperature programmed desorption experiments [15], since they yield too high desorption barriers for both mechanisms. Using periodic CCSD(T), however, we find that desorption barriers for the two mechanisms are very close and agree rather well with the experimental estimate of 2.5 ± 0.1 eV. Furthermore, CCSD(T) desorption energies are 2.62 and 2.67 eV for the H2 and H2* mechanisms. DFT-PBE predicts desorption energies of 1.95 and 2.14 eV, respectively, vastly misjudging the absolute magnitude, as well as the relative difference of the desorption barrier for the two mechanisms. The SCAN functional improves the PBE desorption barriers, however, only by ameliorating the description of the chemisorption energy and not of the adsorption barrier. Hybrid functional results are in satisfactory agreement with CSSD(T). Moreover, PBE0 and HSE06 estimated desorption energies are 2.43 and 2.38 eV for the H2 mechanism and 2.47 and 2.44 eV for the H2* one. We stress that the two desorption energies are not only significantly higher than the DFT-PBE ones but also not far from each other. B3LYP yields desorption energies of 2.50 and 2.66 eV for the H2 and H2* mechanisms respectively. Although the energies are close to the experimental estimate we note that the overall picture for

the reaction mechanism is significantly different than the CCSD(T) one. The H2 pathway is much prefered over the H2* one due to the mistreatment of the relative difference of the two adsorption barriers, stemming from the LDA part of the exchange-correlation functional. Finally the RPA desorption energies, although they represent a significant improvement over DFT-PBE, they still inherit shortcomings of the parent PBE density functional, by favoring the H2 adsorption channel.

Summary.—We have performed a range of DFT and quantum chemical wavefunction based calculations for the H2 and H2* adsorption/desorption mechanisms of H_2 on the Si(100) surface at low coverage. We show that periodic CCSD(T) calculations yield excellent agreement with experimental results for the adsorption barriers and the reaction energy. In contrast to previous calculations, we find similar activation energies for the H2 and H2* adsorption mechanisms. DFT-GGA and DFT-meta-GGA functionals over-stabilize the H2 adsorption mechanism due to incorrect ground state densities caused by self-interaction errors. We argue that both a correct description of the H_2 molecule dissociation, as well as of the surface dimer reconstruction is essential for a precise interpretation of the reaction mechanisms. We note that hybrid functionals, like PBE0 and HSE06 slightly underestimate the adsorption barriers, however, they yield adequate results for the energetics of the reaction. We have demonstrated that high level periodic wavefunction based methods have the potential to serve as accurate benchmark theories for predicting reaction energetics on periodic surfaces, which will ultimately help to further improve upon computationally more efficient yet less accurate methods.

This project has received funding from the European Research Council (ERC) under the European Union's Horizon 2020 research and innovation program (grant agreement No 715594). The computational results presented here were conducted on the IBM iDataPlex HPC system HYDRA of the Max Planck Computing and Data Facility (MPCDF).

* andreas.grueneis@tuwien.ac.at

[1] W. Kohn and L. J. Sham, Phys. Rev. **140**, A1133 (1965).
[2] G.-J. Kroes, Progress in Surface Science **60**, 1 (1999).
[3] A. Gross, *Theoretical surface science*, Vol. 1 (Springer, 2014).
[4] A. J. Cohen, P. Mori-Sánchez, and W. Yang, Chem. Rev. **112**, 289 (2012).
[5] L. Schimka, J. Harl, A. Stroppa, A. Grüneis, M. Marsman, F. Mittendorfer, and G. Kresse, Nature Materials **9**, 741 (2010).
[6] J. P. Perdew and A. Zunger, Phys. Rev. B **23**, 5048 (1981).
[7] T. Helgaker, P. Jørgensen, and J. Olsen, *Molecular Electronic-Structure Theory* (Wiley, 2000).
[8] J. Zheng, Y. Zhao, and D. G. Truhlar, Journal of Chemical Theory and Computation **5**, 808 (2009).
[9] G. H. Booth, A. Grüneis, G. Kresse, and A. Alavi, Nature **493**, 365 (2013).
[10] J. Yang, W. Hu, D. Usvyat, D. Matthews, M. Schütz, and G. K.-L. Chan, Science **345**, 640 (2014).
[11] E. Voloshina, D. Usvyat, M. Schutz, Y. Dedkov, and B. Paulus, Phys. Chem. Chem. Phys. **13**, 12041 (2011).
[12] F. Libisch, C. Huang, P. Liao, M. Pavone, and E. A. Carter, Phys. Rev. Lett. **109**, 198303 (2012).
[13] A. Kubas, D. Berger, H. Oberhofer, D. Maganas, K. Reuter, and F. Neese, The Journal of Physical Chemistry Letters **7**, 4207 (2016).
[14] A. D. Boese and J. Sauer, Journal of Computational Chemistry **37**, 2374 (2016).
[15] U. Höfer, L. Li, and T. F. Heinz, Phys. Rev. B **45**, 9485 (1992).
[16] E. Pehlke and M. Scheffler, Phys. Rev. Lett. **74**, 952 (1995).
[17] M. R. Radeke and E. A. Carter, Phys. Rev. B **54**, 11803 (1996).
[18] A. Gross, M. Bockstedte, and M. Scheffler, Phys. Rev. Lett. **79**, 701 (1997).
[19] A. Biedermann, E. Knoesel, Z. Hu, and T. F. Heinz, Phys. Rev. Lett. **83**, 1810 (1999).
[20] E. Penev, P. Kratzer, and M. Scheffler, The Journal of Chemical Physics **110**, 3986 (1999).
[21] M. Dürr, M. B. Raschke, E. Pehlke, and U. Höfer, Phys. Rev. Lett. **86**, 123 (2001).
[22] M. B. Raschke and U. Höfer, Phys. Rev. B **63**, 201303 (2001).
[23] J. A. Steckel, T. Phung, K. D. Jordan, and P. Nachtigall, The Journal of Physical Chemistry B **105**, 4031 (2001).
[24] C. Filippi, S. B. Healy, P. Kratzer, E. Pehlke, and M. Scheffler, Phys. Rev. Lett. **89**, 166102 (2002).
[25] M. Dürr and U. Höfer, Surface Science Reports **61**, 465 (2006).
[26] W. Brenig and E. Pehlke, Progress in Surface Science **83**, 263 (2008).
[27] R. A. Wolkow, Phys. Rev. Lett. **68**, 2636 (1992).
[28] A. Ramstad, G. Brocks, and P. J. Kelly, Phys. Rev. B **51**, 14504 (1995).
[29] S. B. Healy, C. Filippi, P. Kratzer, E. Penev, and M. Scheffler, Phys. Rev. Lett. **87**, 016105 (2001).
[30] F. Hummel, T. Tsatsoulis, and A. Grüneis, The Journal of Chemical Physics **146**, 124105 (2017).
[31] T. Tsatsoulis, F. Hummel, D. Usvyat, M. Schütz, G. H. Booth, S. S. Binnie, M. J. Gillan, D. Alfè, A. Michaelides, and A. Grüneis, The Journal of Chemical Physics **146**, 204108 (2017).
[32] T. Gruber, K. Liao, T. Tsatsoulis, F. Hummel, and A. Grüneis, Phys. Rev. X **8**, 021043 (2018).
[33] J. P. Perdew, K. Burke, and M. Ernzerhof, Phys. Rev. Lett. **77**, 3865 (1996).
[34] G. Henkelman and H. Jónsson, The Journal of Chemical Physics **113**, 9978 (2000).
[35] G. Kresse and J. Hafner, Journal of Physics: Condensed Matter **6**, 8245 (1994).
[36] G. Kresse and J. Furthmüller, Computational Materials Science **6**, 15 (1996).
[37] G. Kresse and J. Furthmüller, Phys. Rev. B **54**, 11169 (1996).
[38] P. E. Blöchl, Phys. Rev. B **50**, 17953 (1994).
[39] G. Kresse and D. Joubert, Phys. Rev. B **59**, 1758 (1999).

[40] J. P. Perdew and K. Schmidt, AIP Conference Proceedings **577**, 1 (2001).
[41] T. H. Dunning, The Journal of Chemical Physics **90**, 1007 (1989).
[42] D. Feller, Journal of Computational Chemistry **17**, 1571 (1996).
[43] K. L. Schuchardt, B. T. Didier, T. Elsethagen, L. Sun, V. Gurumoorthi, J. Chase, J. Li, and T. L. Windus, Journal of Chemical Information and Modeling **47**, 1045 (2007).
[44] G. H. Booth, T. Tsatsoulis, G. K.-L. Chan, and A. Grüneis, The Journal of Chemical Physics **145**, 084111 (2016).
[45] J. Sun, A. Ruzsinszky, and J. P. Perdew, Phys. Rev. Lett. **115**, 036402 (2015).
[46] J. Sun, R. C. Remsing, Y. Zhang, Z. Sun, A. Ruzsinszky, H. Peng, Z. Yang, A. Paul, U. Waghmare, X. Wu, M. L. Klein, and J. P. Perdew, Nature Chemistry **8**, 831 (2016).
[47] A. D. Becke, The Journal of Chemical Physics **98**, 5648 (1993).
[48] C. Adamo and V. Barone, The Journal of Chemical Physics **110**, 6158 (1999).
[49] A. V. Krukau, O. A. Vydrov, A. F. Izmaylov, and G. E. Scuseria, The Journal of Chemical Physics **125**, 224106 (2006).
[50] J. Harl, L. Schimka, and G. Kresse, Phys. Rev. B **81**, 115126 (2010).
[51] X. Ren, P. Rinke, C. Joas, and M. Scheffler, Journal of Materials Science **47**, 7447 (2012).
[52] F. Furche, Phys. Rev. B **64**, 195120 (2001).
[53] T. Helgaker, T. A. Ruden, P. Jørgensen, J. Olsen, and W. Klopper, Journal of Physical Organic Chemistry **17**, 913 (2004).
[54] A. Grüneis, M. Marsman, and G. Kresse, The Journal of Chemical Physics **133**, 074107 (2010).
[55] D. Porezag and M. R. Pederson, The Journal of Chemical Physics **102**, 9345 (1995).
[56] A. Mahler, B. G. Janesko, S. Moncho, and E. N. Brothers, The Journal of Chemical Physics **146**, 234103 (2017).
[57] M.-C. Kim, E. Sim, and K. Burke, Phys. Rev. Lett. **111**, 073003 (2013).
[58] B. G. Janesko and G. E. Scuseria, The Journal of Chemical Physics **128**, 244112 (2008).
[59] A. Patra, J. Sun, and J. P. Perdew, arXiv preprint arXiv:1807.05450 (2018).
[60] E. Solomonik, D. Matthews, J. R. Hammond, J. F. Stanton, and J. Demmel, Journal of Parallel and Distributed Computing **74**, 3176 (2014), domain-Specific Languages and High-Level Frameworks for High-Performance Computing.
[61] G. Henkelman, B. P. Uberuaga, and H. Jónsson, The Journal of Chemical Physics **113**, 9901 (2000).
[62] A. Grüneis, G. H. Booth, M. Marsman, J. Spencer, A. Alavi, and G. Kresse, Journal of Chemical Theory and Computation **7**, 2780 (2011).
[63] J. Harl and G. Kresse, Phys. Rev. B **77**, 045136 (2008).
[64] J. Harl and G. Kresse, Phys. Rev. Lett. **103**, 056401 (2009).

Supplemental material - Reaction energetics of Hydrogen on Si(100) surface revisited: A periodic many-electron theory study

All electronic structure theory calculations discussed below have been conducted using the VASP code with PAW potentials [36, 37, 39] and an interface to the coupled cluster code CC4S employing the Cyclops Tensor Framework (CTF) [60].

The minimum energy paths of intra- and inter-dimer reactions are determined using the nudged elastic band (NEB) method within variational transition state theory [34]. We used 8 images for the calculations. For the electronic structure calculations we used the PBE functional. One-electron states were expanded using a plane-wave basis with a cutoff energy of 250 eV, alongside an $8 \times 8 \times 1$ k-mesh to sample the first Brillouin zone. The exact energies of the transition states are determined by an interpolation or by using the the climbing NEB method [61]. The structures for the intial state, the two transition states (corresponding to the two different pathways), and the final state are given in the end of the supplementary in VASP format.

We now discuss the convergence of the adsorption barriers and the reaction energy, at different levels of theory, with respect to parameters such as the k-point sampling of the first Brillouin zone and the basis set. Plane-waves were used throughout all calculations. The electronic states of the H atoms were treated as valence states while the 1s, 2s, and 2p states of the Si atoms were kept frozen. For wave-function-based correlated calculations we employ canonical HF orbitals for the occupied electron states, expanded using a 500 eV plane-wave energy cutoff. Unoccupied one-electron states are constructed using Dunning's contracted aug-cc-pVQZ-g (without g angular momentum functions) basis set [41–43] mapped onto a plane-wave representation [44]. We always rediagonalize the Fock matrix in order to perform a canonical correlated calculation. Since the aVQZ consists of 2572 virtual orbital states, we further reduce the number of unoccupied states using MP2 natural orbitals (NOs), obtained from the virtual–virtual orbital block diagonalization (made up from the aVQZ basis set) of the one-electron reduced density matrix at the level of MP2 [62]. A $2 \times 2 \times 1$ and a $4 \times 4 \times 1$ k-mesh was employed for the twist-averaging procedure [32] in MP2 and CCSD calculations, whereas the remaining finite size error of the correlation energy was corrected for using an interpolation technique of the structure factor on a plane-wave grid [32]. CCSD calculations further utilize a tensor rank decomposition technique for the electron integrals as outlined in Ref. 30.

We first discuss the basis set convergence of the adsorption barriers (E_{ads}) and the reaction energy (E_{rxn}),

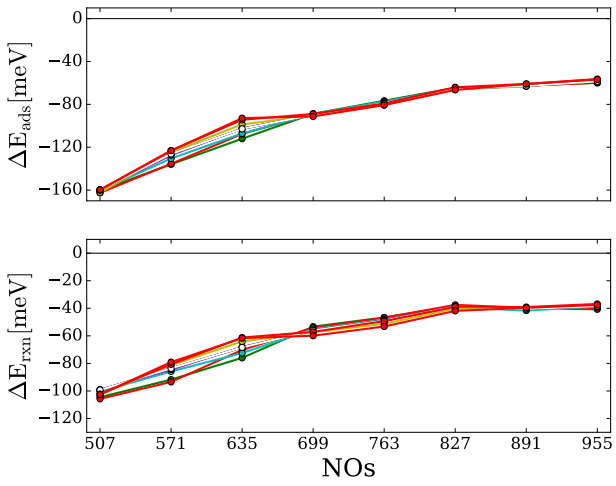

FIG. 3. MP2 basis set convergence with respect to the number of NOs for the adsorption barrier (for the inter-dimer path) and the reaction energy. Each line corresponds to a different k-point in the Brillouin zone of the $4 \times 4 \times 1$ k-mesh. The energies are plotted as the difference from the MP2 value obtained using the full aVQZ–g PGTOs basis set. All energies in meV.

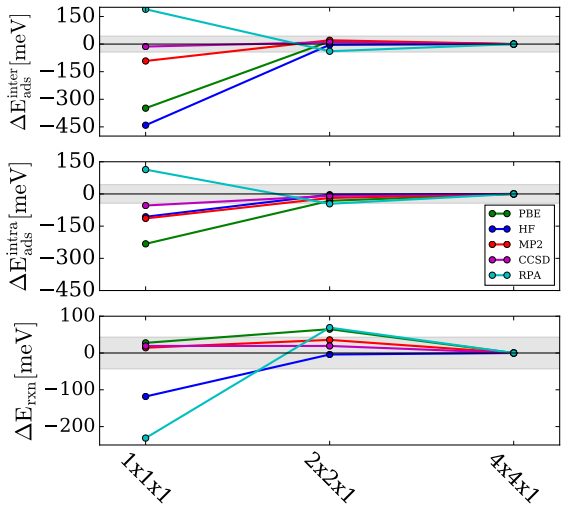

FIG. 4. Dependence of the adsorption barriers for the two pathways and the reaction energy with respect to the k-mesh size. For MP2 and CCSD, we perform twist-averaged calculations for the $2 \times 2 \times 1$ and $4 \times 4 \times 1$ k-meshes. Only the convergence of the correlation part of the energy is shown for MP2 and CCSD, using 768 NOs. The energies are shown as the difference from the $4 \times 4 \times 1$ value for each method. The shaded region denotes the 1 kcal/mol area from the reference value. All energies in meV.

defined as

$$E_{\text{rxn}} = E_{\text{initial}} - E_{\text{final}}, \tag{A.1}$$

and

$$E_{\text{ads}} = E_{\text{transition}} - E_{\text{initial}}, \tag{A.2}$$

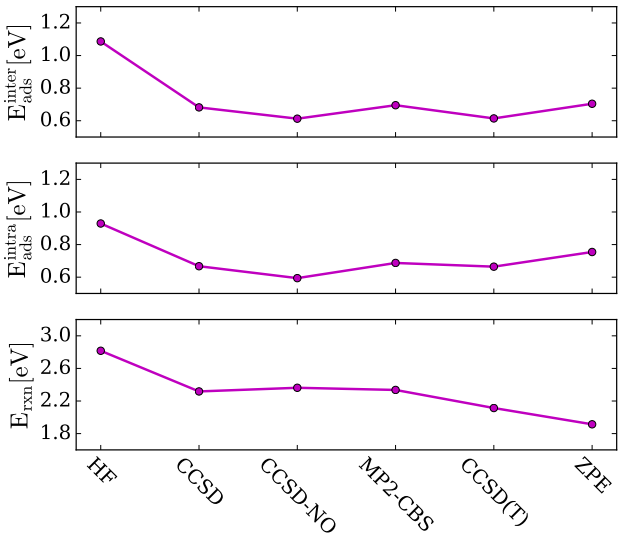

FIG. 5. Different contributions to the CCSD(T) adsorption barriers and reaction energy. Starting from left to right we add the contributions to the adsorption barriers and the reaction energy. Thus, the ZPE contribution constitutes the final CCSD(T) number. Each contribution is defined in the text. We start from HF, add the CCSD correlation energy, two basis set corrections (one based on CCSD and one on the CBS MP2), the perturbative triples correction (T), and finally the ZPE. All energies given in eV.

respectively. In Fig. 3 we show the convergence of the MP2 correlation energy of the different 10 k-points, corresponding to a $4 \times 4 \times 1$ k-mesh, with respect to the number of NOs. The NOs are obtained from the diagonalization of the virtual–virtual block of the one-electron MP2 reduced density matrix, using the aVQZ-g virtual states. The adsorption barriers and the reaction energy are plotted as the difference from the MP2 result, using the full aVQZ-g one-electron virtual states. We observe a very similar behavior for all k-shifts of both the barriers and the reaction energy. In particular, we have the same basis set error for all k-shifts when we use 699 virtual NOs within a few meV. We conclude that a large basis set calculation is only need for the Γ-point, since all other k-shifts exhibit the same basis set convergence. The aVQZ-g basis set limit result within a twist-averaged $4 \times 4 \times 1$ k-mesh at the MP2 level can thus be obtained as

$$E_{\text{MP2}} = E^{4\times4\times1}_{\text{MP2-699NOs}} + \Delta E^{1\times1\times1}_{\text{MP2-aVQZ-g}}. \tag{A.3}$$

We stress that the aVQZ-g virtual orbital set still includes a basis set incompleteness and superposition error. We add a further correction $\Delta E^{1\times1\times1}_{\text{dMP2-PW}}$ which is the difference of the direct MP2 (dMP2) Γ-point calculation using the full plane-wave virtual states (35076 states) and the dMP2 aVQZ-g calculation. Thus the converged

MP2 results are obtained via the formula

$$E_{\mathrm{MP2}} = E^{4\times4\times1}_{\mathrm{MP2\text{-}699NOs}} + \Delta E^{1\times1\times1}_{\mathrm{MP2\text{-}aVQZ\text{-}g}} + \Delta E^{1\times1\times1}_{\mathrm{dMP2\text{-}PW}}. \tag{A.4}$$

Similarly, RPA calculations were performed with the VASP code [63, 64], using PBE orbitals as a reference, a full $4\times4\times1$ k-mesh, and the aVQZ-g virtual orbital states with a Γ-point basis set correction using the full plane-wave virtual states. Consequently, the converged RPA correlation energy is computed as

$$E_{\mathrm{RPA}} = E^{4\times4\times1}_{\mathrm{RPA\text{-}aVQZ\text{-}g}} + \Delta E^{1\times1\times1}_{\mathrm{RPA\text{-}PW}}. \tag{A.5}$$

We now turn to the discussion of the convergence of the MP2 and CCSD correlation energies with respect to the k-point sampling of the Brillouin zone via the twist-averaging technique. The CCSD correlation energy for the $4\times4\times1$ k-mesh is calculated as

$$E_{\mathrm{CCSD}} = E^{4\times4\times1}_{\mathrm{CCSD\text{-}699NOs}} + \Delta E^{1\times1\times1}_{\mathrm{CCSD\text{-}1377NOs}} + \Delta E^{1\times1\times1}_{\mathrm{dMP2\text{-}PW}}, \tag{A.6}$$

where $E^{4\times4\times1}_{\mathrm{CCSD\text{-}699NOs}}$ is the twist-averaged finite-size corrected CCSD correlation energy using 699 virtual NOs, $\Delta E^{1\times1\times1}_{\mathrm{CCSD\text{-}1275NOs}}$ is a basis set correction based on a Γ-point CCSD calculation using 1275 NOs, and $\Delta E^{1\times1\times1}_{\mathrm{dMP2\text{-}PW}}$ is the CBS limit correction and is defined as

$$\Delta E^{1\times1\times1}_{\mathrm{dMP2\text{-}PW}} = E^{1\times1\times1}_{\mathrm{dMP2\text{-}PW}} - E^{1\times1\times1}_{\mathrm{dMP2\text{-}1377NOs}}. \tag{A.7}$$

The convergence of PBE, HF, MP2, and CCSD with respect to the k-point sampling is shown in Fig. 4. It is safe to presume that the results are converged well within 1 kcal/mol (chemical accuracy) using a $4\times4\times1$ twist-averaged k-point sampling with MP2 and CCSD. PBE and HF energies can be obtained using a denser k-mesh, and we have checked convergence with respect to the $4\times4\times1$ mesh.

Finally we estimate the perturbative triples correction in CCSD by performing a Γ-point calculation with a few virtual NOs (251). The CCSD(T) barriers and reaction energy are obtained via the formula

$$E_{\mathrm{CCSD(T)}} = E^{4\times4\times1}_{\mathrm{CCSD\text{-}699NOs}} + \Delta E^{1\times1\times1}_{\mathrm{CCSD\text{-}1377NOs}} + \Delta E^{1\times1\times1}_{\mathrm{dMP2\text{-}PW}} + \Delta E^{1\times1\times1}_{\mathrm{CCSD(T)\text{-}251NOs}}, \tag{A.8}$$

where $\Delta E^{1\times1\times1}_{\mathrm{CCSD(T)\text{-}251NOs}}$ is defined as

$$\Delta E^{1\times1\times1}_{\mathrm{CCSD(T)\text{-}251NOs}} = E^{1\times1\times1}_{\mathrm{CCSD(T)\text{-}251NOs}} - E^{1\times1\times1}_{\mathrm{CCSD\text{-}251NOs}}. \tag{A.9}$$

TABLE II. Convergence of the CCSD(T) energy for the two adsorption barriers, the desorption energy, and the reaction energy with respect to the NOs used for the (T) correction ($\Delta E^{1\times1\times1}_{\mathrm{CCSD(T)\text{-}NOs}}$). All contributions from Fig. 5 are included.

# of NOs	E_a^{ads}[H2]	E_a^{ads}[H2*]	E_a^{des}	E_{rxn}
123	0.75	0.80	2.73	1.98
187	0.74	0.79	2.66	1.92
251	0.70	0.75	2.62	1.91

The different contributions to the CCSD(T) energies are shown in Fig. 5 for the two barriers and the reaction energy. These contributions are the HF energy and the CCSD(T) energy as defined in Eq. (A.8). The convergence of this final CCSD(T) energies with respect to the number of NOs used to evaluate $\Delta E^{1\times1\times1}_{\mathrm{CCSD(T)\text{-}NOs}}$ is shown in Table 1.

```
   H2Si Initial State
   3.86430683876830
   2.0000000000000000   0.0000000000000000   0.0000000000000000
   0.0000000000000000   2.0000000000000000   0.0000000000000000
   0.0000000000000000   0.0000000000000000   6.0000000000000000
   Si  H
32  10
Selective dynamics
Direct
  0.2500000000000000  0.2500000000000000  0.2178511306643500 F F F
  0.2500000000000000  0.7500000000000000  0.2178511306643500 F F F
  0.7500000000000000  0.2500000000000000  0.2178511306643500 F F F
  0.7500000000000000  0.7500000000000000  0.2178511306643500 F F F
  0.2500000000000000  0.0000000000000000  0.2767766922712340 F F F
  0.2500000000000000  0.5000000000000000  0.2767766922712340 F F F
  0.7500000000000000  0.0000000000000000  0.2767766922712340 F F F
  0.7500000000000000  0.5000000000000000  0.2767766922712340 F F F
  0.0000000000000000  0.0000000000000000  0.3357022613286986 F F F
  0.0000000000000000  0.5000000000000000  0.3357022613286986 F F F
  0.5000000000000000  0.0000000000000000  0.3357022613286986 F F F
  0.5000000000000000  0.5000000000000000  0.3357022613286986 F F F
  0.9978920774748270  0.2501002369370171  0.3947633070601618 T T T
  0.9914559619550580  0.7499512933309244  0.3945982431302275 T T T
  0.5083137146876741  0.2501333199380792  0.3946198887123143 T T T
  0.5019440374483743  0.7499674324913221  0.3947389619840295 T T T
  0.2541119277327683  0.2502905986368278  0.4493732331770072 T T T
  0.2457453603112742  0.7499310306516059  0.4493390251790675 T T T
  0.7537242105456929  0.2503514510486242  0.4579837457055499 T T T
  0.7460896440207401  0.7501790623329722  0.4579492735333748 T T T
  0.2498791406554453  0.0000732209586753  0.5069393452617033 T T T
  0.2498260414210869  0.5001676733342216  0.5072306477502692 T T T
  0.7498233725809779  0.0002333884679654  0.5189430497828482 T T T
  0.7499466120632379  0.5003731836349984  0.5191022580660728 T T T
  0.4860978039951767  0.0142582256468318  0.5733764528846966 T T T
  0.4863854241659687  0.4851213218582255  0.5737136797344280 T T T
  0.0135649641097707  0.9859358840497386  0.5733331221742625 T T T
  0.0133676923075392  0.5161080926144457  0.5737177839672417 T T T
  0.1295234754652361  0.2509433044909413  0.6043442185191165 T T T
  0.4185550465760738  0.2493861625438807  0.6374110663955688 T T T
  0.0803636886906659  0.7513636252533308  0.6377607193825289 T T T
  0.3696180468338684  0.7497450248524198  0.6046676824393655 T T T
  0.1006049997488745  0.2500000000000000  0.1776316733665411 F F F
  0.3992252435132997  0.2500000000000000  0.1775467218254292 F F F
  0.1006049997488745  0.7500000000000000  0.1776316733665411 F F F
  0.3992252435132997  0.7500000000000000  0.1775467218254292 F F F
  0.6008289119501029  0.2500000000000000  0.1775120046712431 F F F
  0.8995143750959684  0.2500000000000000  0.1776836850124539 F F F
  0.6008289119501029  0.7500000000000000  0.1775120046712431 F F F
  0.8995143750959684  0.7500000000000000  0.1776836850124539 F F F
  0.4054765258197098  0.5756991667299082  0.7687658977059009 T T T
  0.4182959262467486  0.4945716077148358  0.7513786008775105 T T T
```

```
   H2Si Inter-transition
   3.86430683876830
     2.0000000000000000    0.0000000000000000    0.0000000000000000
     0.0000000000000000    2.0000000000000000    0.0000000000000000
     0.0000000000000000    0.0000000000000000    6.0000000000000000
   Si   H
    32    10
Selective dynamics
Direct
  0.2500000000000000  0.2500000000000000  0.2178511306643500   F   F   F
  0.2500000000000000  0.7500000000000000  0.2178511306643500   F   F   F
  0.7500000000000000  0.2500000000000000  0.2178511306643500   F   F   F
  0.7500000000000000  0.7500000000000000  0.2178511306643500   F   F   F
  0.2500000000000000  0.0000000000000000  0.2767766922712341   F   F   F
  0.2500000000000000  0.5000000000000000  0.2767766922712341   F   F   F
  0.7500000000000000  0.0000000000000000  0.2767766922712341   F   F   F
  0.7500000000000000  0.5000000000000000  0.2767766922712341   F   F   F
  0.0000000000000000  0.0000000000000000  0.3357022613286986   F   F   F
  0.0000000000000000  0.5000000000000000  0.3357022613286986   F   F   F
  0.5000000000000000  0.0000000000000000  0.3357022613286986   F   F   F
  0.5000000000000000  0.5000000000000000  0.3357022613286986   F   F   F
  0.9970521248262706  0.2476116137412846  0.3946217310396840   T   T   T
  0.9936822501531496  0.7520561768733628  0.3945119891604291   T   T   T
  0.5065651667398511  0.2493485117389162  0.3946624882248159   T   T   T
  0.5019674902428138  0.7509705936117446  0.3948196382776604   T   T   T
  0.2520963790179814  0.2463219653440258  0.4496448387907274   T   T   T
  0.2466788381548096  0.7539758841158494  0.4502220790198872   T   T   T
  0.7525163846941552  0.2467526613717999  0.4574976140632035   T   T   T
  0.7478807245835398  0.7525080608218051  0.4569523105562249   T   T   T
  0.2563735796420387  0.0019746272349974  0.5108128261939918   T   T   T
  0.2449607266672484  0.4989416507573006  0.5048840054958662   T   T   T
  0.7500798859412643  0.9985998132712952  0.5201522387184853   T   T   T
  0.7532286599949596  0.5004219100137551  0.5157062628224663   T   T   T
  0.4915343508783619  0.0007328805845182  0.5785304218449727   T   T   T
  0.4867546152479328  0.4940532216450972  0.5657493201394315   T   T   T
  0.0130579997065171  0.9815966228046186  0.5747208643540517   T   T   T
  0.0104878373275742  0.5182846071859749  0.5722534550904741   T   T   T
  0.1177869452184272  0.2513571754410759  0.6030794345535369   T   T   T
  0.4155246954615945  0.2642396086117805  0.6282573495443666   T   T   T
  0.0763412421882709  0.7460855784749263  0.6394320917066870   T   T   T
  0.3851200580817243  0.7342800762848545  0.6180752622274410   T   T   T
  0.1006049997488745  0.2500000000000000  0.1776316733665411   F   F   F
  0.3992252435132997  0.2500000000000000  0.1775467218254292   F   F   F
  0.1006049997488745  0.7500000000000000  0.1776316733665411   F   F   F
  0.3992252435132997  0.7500000000000000  0.1775467218254292   F   F   F
  0.6008289119501029  0.2500000000000000  0.1775120046712431   F   F   F
  0.8995143750959684  0.2500000000000000  0.1776836850124540   F   F   F
  0.6008289119501029  0.7500000000000000  0.1775120046712431   F   F   F
  0.8995143750959684  0.7500000000000000  0.1776836850124540   F   F   F
  0.4371319861066793  0.5814523912550201  0.6840055911338208   T   T   T
  0.4371388353329146  0.4661507452574352  0.6857069372556538   T   T   T
```

```
   H2Si Intra-transition
   3.86430683876830
     2.0000000000000000    0.0000000000000000    0.0000000000000000
     0.0000000000000000    2.0000000000000000    0.0000000000000000
     0.0000000000000000    0.0000000000000000    6.0000000000000000
   Si   H
    32    10
Selective dynamics
Direct
  0.2500000000000000  0.2500000000000000  0.2178511306643500   F   F   F
  0.2500000000000000  0.7500000000000000  0.2178511306643500   F   F   F
  0.7500000000000000  0.2500000000000000  0.2178511306643500   F   F   F
  0.7500000000000000  0.7500000000000000  0.2178511306643500   F   F   F
  0.2500000000000000  0.0000000000000000  0.2767766922712341   F   F   F
  0.2500000000000000  0.5000000000000000  0.2767766922712341   F   F   F
  0.7500000000000000  0.0000000000000000  0.2767766922712341   F   F   F
  0.7500000000000000  0.5000000000000000  0.2767766922712341   F   F   F
  0.0000000000000000  0.0000000000000000  0.3357022613286986   F   F   F
  0.0000000000000000  0.5000000000000000  0.3357022613286986   F   F   F
  0.5000000000000000  0.0000000000000000  0.3357022613286986   F   F   F
  0.5000000000000000  0.5000000000000000  0.3357022613286986   F   F   F
  0.9973366608778949  0.2500000801794383  0.3946813338223449   T   T   T
  0.9931277971823532  0.7499999819979261  0.3947453840155005   T   T   T
  0.5076623539448453  0.2499999791901445  0.3947149473314026   T   T   T
  0.5032427143456849  0.7499999448621247  0.3945127659685829   T   T   T
  0.2529441974381704  0.2499998503040353  0.4494116446603049   T   T   T
  0.2483031430590528  0.7500001189705909  0.4494829258344244   T   T   T
  0.7532023853785577  0.2500000087130616  0.4580048810371303   T   T   T
  0.7468052988003065  0.7500001152885148  0.4576659801614334   T   T   T
  0.2490786580303400  0.9994739886576217  0.5068019182800327   T   T   T
  0.2490785565744022  0.5005260242159526  0.5068020475872209   T   T   T
  0.7488846946478996  0.9995277195559314  0.5189133785931902   T   T   T
  0.7488847217895653  0.5004721465623295  0.5189134336956376   T   T   T
  0.4846076780017386  0.0127530697818007  0.5732239641490573   T   T   T
  0.4846076089274498  0.4872472156831404  0.5732239039035931   T   T   T
  0.0148383971035849  0.9814521955441114  0.5721350644733337   T   T   T
  0.0148384490024012  0.5185478993520343  0.5721349867230389   T   T   T
  0.1079548834149076  0.2499998641166161  0.6100014464225474   T   T   T
  0.4173391751179492  0.2499998823638762  0.6360643817680882   T   T   T
  0.0797018358064009  0.7500000471873380  0.6371761518674145   T   T   T
  0.3667380721235752  0.7499998269529726  0.6036402370790296   T   T   T
  0.1006049997488745  0.2500000000000000  0.1776316733665411   F   F   F
  0.3992252435132997  0.2500000000000000  0.1775467218254292   F   F   F
  0.1006049997488745  0.7500000000000000  0.1776316733665411   F   F   F
  0.3992252435132997  0.7500000000000000  0.1775467218254292   F   F   F
  0.6008289119501029  0.2500000000000000  0.1775120046712431   F   F   F
  0.8995143750959684  0.2500000000000000  0.1776836850124540   F   F   F
  0.6008289119501029  0.7500000000000000  0.1775120046712431   F   F   F
  0.8995143750959684  0.7500000000000000  0.1776836850124540   F   F   F
  0.1874924005432522  0.2500000073252465  0.6807275954718290   T   T   T
  0.0571553050475907  0.2499999786148833  0.6807061273942255   T   T   T
```

```
   H2Si Final
   3.86430683876830
   2.0000000000000000   0.0000000000000000   0.0000000000000000
   0.0000000000000000   2.0000000000000000   0.0000000000000000
   0.0000000000000000   0.0000000000000000   6.0000000000000000
   Si  H
32  10
Selective dynamics
Direct
  0.2500000000000000  0.2500000000000000  0.2178511306643500 F F F
  0.2500000000000000  0.7500000000000000  0.2178511306643500 F F F
  0.7500000000000000  0.2500000000000000  0.2178511306643500 F F F
  0.7500000000000000  0.7500000000000000  0.2178511306643500 F F F
  0.2500000000000000  0.0000000000000000  0.2767766922712340 F F F
  0.2500000000000000  0.5000000000000000  0.2767766922712340 F F F
  0.7500000000000000  0.0000000000000000  0.2767766922712340 F F F
  0.7500000000000000  0.5000000000000000  0.2767766922712340 F F F
  0.0000000000000000  0.0000000000000000  0.3357022613286986 F F F
  0.0000000000000000  0.5000000000000000  0.3357022613286986 F F F
  0.5000000000000000  0.0000000000000000  0.3357022613286986 F F F
  0.5000000000000000  0.5000000000000000  0.3357022613286986 F F F
  0.9967247900399892  0.2500008869468627  0.3944560275893023 T T T
  0.9949995669207292  0.7500000934871268  0.3948835224892601 T T T
  0.5074169807155093  0.2499962226927760  0.3943600233409091 T T T
  0.5031410894650846  0.7500022522586248  0.3948900877130442 T T T
  0.2527381720431977  0.2499986500474608  0.4487189339452072 T T T
  0.2488535739353010  0.7500030761744489  0.4506066275498521 T T T
  0.7521190857856491  0.2500005267809053  0.4577236604093188 T T T
  0.7484203614488777  0.7500064126715218  0.4574694825931995 T T T
  0.2455568333529209  0.0020370677618386  0.5069250081617875 T T T
  0.2455451787282528  0.4979618269643509  0.5069208380859964 T T T
  0.7523123601027288  0.9994164067969300  0.5185723931509145 T T T
  0.7522972063022922  0.5005860972992371  0.5185689029181350 T T T
  0.4862180067169950  0.0062173190082292  0.5716045732131283 T T T
  0.4861998279522483  0.4937973799485066  0.5716025146509965 T T T
  0.0151441151947269  0.9932392813463180  0.5735649325969819 T T T
  0.0151332883472283  0.5067171811708249  0.5735604045455229 T T T
  0.0847592334991161  0.2499795857123008  0.6244812988807741 T T T
  0.3964364730670507  0.2500088252499786  0.6256133457520556 T T T
  0.0715436901136677  0.7499756180826548  0.6348832855432121 T T T
  0.3573219973930112  0.7500084857447613  0.6040802452993346 T T T
  0.1006049997488745  0.2500000000000000  0.1776316733665411 F F F
  0.3992252435132997  0.2500000000000000  0.1775467218254292 F F F
  0.1006049997488745  0.7500000000000000  0.1776316733665411 F F F
  0.3992252435132997  0.7500000000000000  0.1775467218254292 F F F
  0.6008289119501029  0.2500000000000000  0.1775120046712431 F F F
  0.8995143750959684  0.2500000000000000  0.1776836850124539 F F F
  0.6008289119501029  0.7500000000000000  0.1775120046712431 F F F
  0.8995143750959684  0.7500000000000000  0.1776836850124539 F F F
  0.4704952501322650  0.2500203332986561  0.6857134628054248 T T T
  0.0202614965046356  0.2500020864963545  0.6859279907640059 T T T
```